

VALIDATION OF ANSYS CFX FOR GAS AND LIQUID METAL FLOWS WITH CONJUGATE HEAT TRANSFER WITHIN THE EUROPEAN PROJECT THINS

A. Papukchiev, S. Buchholz

Gesellschaft fuer Anlagen- und Reaktorsicherheit (GRS) gGmbH
Boltzmannstr. 14, 85748 Garching n. Munich, Germany
angel.papukchiev@grs.de; sebastian.buchholz@grs.de

ABSTRACT

Within the FP7 European project THINS (Thermal Hydraulics of Innovative Nuclear Systems), numerical tools for the simulation of the thermal-hydraulics of next generation reactor systems were developed, applied and validated for innovative coolants. The Gesellschaft fuer Anlagen- und Reaktorsicherheit (GRS) gGmbH participated in THINS with activities related to the development and validation of computational fluid dynamics (CFD) and coupled System Thermal Hydraulics (STH) – CFD codes. High quality measurements from the L-STAR and TALL-3D experiments were used to assess the numerical results. Two-equation eddy viscosity and scale resolving turbulence models were used in the validation process of ANSYS CFX for gas and liquid metal flows with conjugate heat transfer. This paper provides a brief overview on the main results achieved at GRS within the project.

KEYWORDS

Innovative reactors, ANSYS CFX, validation

1. INTRODUCTION

Over the last decades, interest has grown amongst the nuclear community for the use of CFD programs for the evaluation of different nuclear reactor safety issues, where traditional analysis tools show deficiencies. Within the FP7 European project THINS, STH, CFD and coupled 1D-3D STH-CFD thermal-hydraulic simulations are being carried out for Generation IV nuclear systems. These are dedicated to the analysis of the thermal-hydraulics of gas, liquid metal and supercritical water cooled reactors. Such innovative fluids represent challenge for the engineers, since these have different properties and behavior from the ones used in the current nuclear facilities.

Within THINS the Gesellschaft fuer Anlagen- und Reaktorsicherheit (GRS) gGmbH participated with activities related to the development and validation of CFD and coupled STH-CFD codes. Emphasis was given to the calculation and analysis of gas and liquid metal experiments. The TALL-3D facility, operated by the KTH Royal Institute of Technology in Stockholm, is designed for thermal-hydraulic experiments with lead-bismuth eutectic (LBE) coolant at natural and forced circulation conditions. In the experiment T01.09 the primary pump is stopped, which leads to a complex transient with local 3D flow and heat transfer phenomena. The thermal-hydraulics in gas cooled reactors has been addressed with the analysis of the L-STAR experiment. The L-STAR test section consists of hexagonal flow channel with an air cooled cylindrical heated rod in its center. Both facilities are well instrumented, and therefore high quality

measurements were used to support the validation of the commercial code ANSYS CFX for advanced coolants. Different turbulence approaches based on RANS (Reynolds-Averaged Navier–Stokes), SAS (Scale Adaptive Simulation) and ZLES (Zonal Large Eddy Simulation) were utilized in the simulations. The objective of this overview paper is to briefly summarize the numerical effort and to highlight only the most significant achievements.

2. L-STAR EXPERIMENT AND ANSYS CFX MODEL DEVELOPMENT

2.1. L-STAR/SL Facility

The L-STAR/SL facility has been designed and constructed at the Karlsruhe Institute of Technology (KIT) in Germany for gas-cooled experiments with single-rod geometries [1]. The air flow in the loop is driven by a single side channel compressor. An isometric view of the facility with its main components is shown in Fig. 1. The coolant in this loop is air at low pressure. The test section in this loop consists of an approx. 3.4 m long hexagonal flow channel with a single cylindrical rod in its center. The cylindrical rod is electrically heated and a large number of thermocouples (TCs) are installed below its surface. The base version of the heater rod is a smooth cylinder with an outer diameter of 35 mm. The flow channel is equipped with two optical windows, which allow access for optical flow measurement methods for velocity field, such as Laser-Doppler Anemometry (LDA). The L-STAR/SL loop instrumentation records mass flow, pressure and temperature at several locations in the pipeline system.

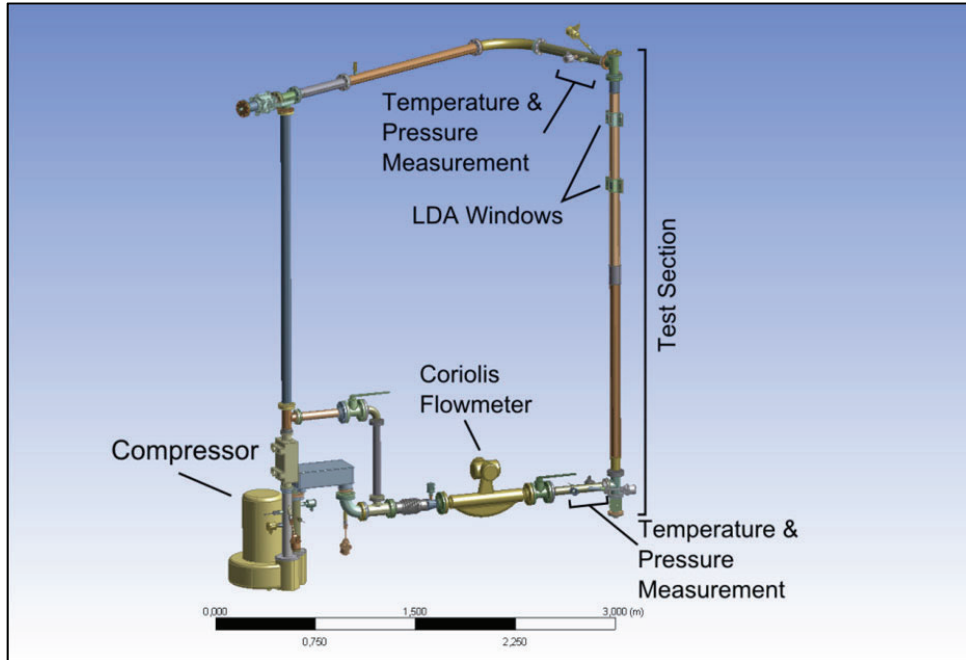


Figure 1. L-STAR Facility.

2.2. ANSYS CFX Model of the L-STAR/SL Facility

Several high quality structured meshes were generated with ICEM CFD and mesh studies were performed, according to OECD/NEA Best Practice Guidelines [2]. The final hexahedral mesh selected for the RANS simulations has 1.5 M elements (min. orthogonality angle 21° , max. aspect ratio 91, max. expansion factor 14). Figure 2 represents the lower and upper parts of the L-STAR/SL test section model. Later, for the scale resolving simulations (SRS) this final mesh was locally refined in order to lower the value of the dimensionless wall distance y^+ down to 0.7.

All steady state calculations were performed with the SST model [3]. Comparative simulations with advanced turbulence models, requiring transient solution were carried out as well: a ZLES and the scale SAS turbulence approaches were selected. Both belong to the so called SRS (Scale Resolving Simulation) models, which resolve the larger eddies, while the small ones are modelled with sub-grid scale models [4]. Since ANSYS CFX Version 14.0 a ZLES model can be used in order to solve a specific part of the CFD domain with complex flow pattern using LES, while the rest of the domain is treated with a RANS turbulence model like SST. Between the RANS and the LES zone there is a so called harmonic flow generator which enforces turbulence fluctuations. In the ZLES calculations the whole test section was within the LES subdomain, whereas the inlet and outlet regions of the facility were simulated with SST.

The SAS model is a new class of unsteady RANS (URANS) models. SAS enforces RANS behavior in stable flow regions and LES behavior in unstable flow regions [4]. The central difference advection scheme was selected for spatial discretization in the SRS simulations. For the time discretization the Second Order Backward Euler scheme has been chosen. For the numerical transport of the quantities (velocity, temperature, etc.) through the solution domain a High Resolution advection scheme was used. Since high rod surface temperatures were observed in the L-STAR experiments, an additional model, which accounts for radiative heat transfer was activated in ANSYS CFX. The time step size in the SRS calculations was chosen within the range $7.5E-5 - 1E-4$ in order to ensure low value of the Courant number.

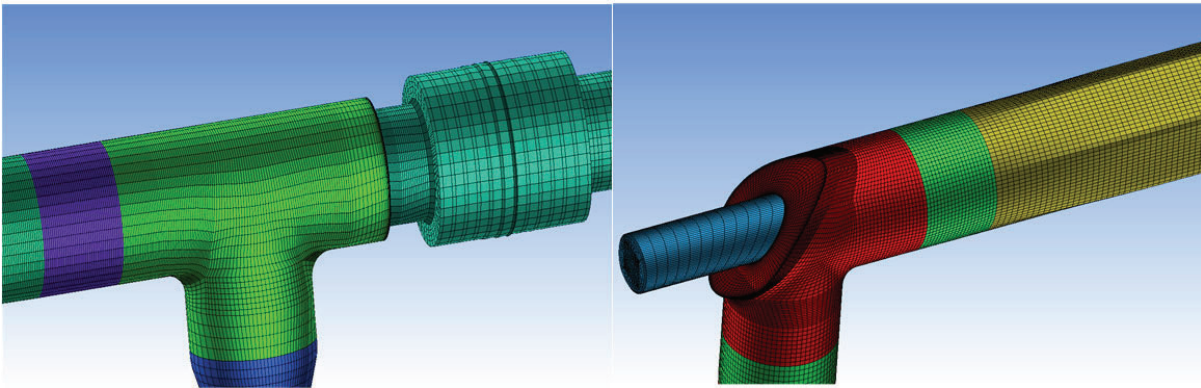


Figure 2. Hexahedral Mesh at Test Section Inlet (left) and Outlet (right).

2.3. Selection of L-STAR/SL Test Cases

Within the scope of the THINS project heated and unheated experiments have been carried out. Moreover, the heat transfer with smooth and ripped rod surfaces was investigated [5]. This paper focuses on the experimental runs with a heated, smooth rod [6]. Inlet mass flow rate and temperature were varied along with the power of the heater, leading to different gas and heater rod surface temperatures. The first steady state simulations showed higher temperatures at the test section outlet than the observed values in the experiment. It was found that these discrepancies are due to heat losses through the test section insulation to the environment, which were not considered in the CFD simulations. Therefore, a heat loss calibration procedure was performed. For each experimental run, the heat losses were calculated and implemented in the CFD model. The boundary conditions of the selected three experimental runs are given in [5] and are summarized in Table I.

Table I. Boundary Conditions for the Experimental Runs with Heated Smooth Rod

Experimental run	Mass flow rate [g/s]	Total heater power [W]	Inlet temp. [°C]	Outlet temp. [°C]	Pressure [bar]	Heat losses [W]
SH-TX-01	24.9	1016	16.3	50.7	1.5	-147.65
SH-TX-02	25.6	677	8.3	32.0	1.5	-61.44
SH-TX-03	25.5	1354	10.3	57.4	1.5	-138.79

3. ANSYS CFX VALIDATION AND DISCUSSION ON THE L-STAR RESULTS

The first objective was to check if the ANSYS CFX calculations with the calibrated input decks represent correctly the global mass and heat balance in the L-STAR/SL test section. Pressure drop and outlet temperature measurements were compared with calculated results. Very small deviations were observed for the outlet temperature (max. $\Delta T_{out} \sim 0.12$ K) and for the pressure drop over the test section (max. $\Delta p \sim 2.5$ Pa). Values for the local rod surface temperature along the rod length were obtained by a set of TCs located in different axial and circumferential locations over the rod length. An increased number of TCs is positioned in the vicinity of the LDA windows. Figures 3 and 4 show the comparison between measured and calculated rod surface temperatures along the rod length. Point zero ($L=0$ mm), chosen by the experimentalists, was positioned close to the top of the rod, which is slightly higher than the perpendicular pipe connected to the test section pipe (see Fig. 1). Therefore, low L (rod length) values should be associated with the upper test section part, while high L values correspond to the lower test section part.

A good agreement between calculations and experiment can be observed in Fig. 3 and Fig. 4. It can be seen, that the temperature of the first measurement point ($L=304$ mm) is lower than the next one ($L=470$ mm). This is due to the fact that the top 300 mm of the rod are not heated. ANSYS CFX captures well the shapes of the axial temperature profiles. Nevertheless, some deviations up to 8 K are present and their location varies in the different experimental runs. The maximum deviation is found in SH-TX-03 at the beginning of the test section. Similar discrepancies (6 K) were observed for the same location in SH-TX-01. Good overall agreement is found for the run SH-TX-02, where the mean deviation from experimental data is 4.6 K. It was found that the influence of the turbulent Prandtl number Pr_t on the RANS results is relatively high. The Pr_t will not influence the temperature at the test section outlet in a steady state experiment, but affects the temperature distribution in the CFD domain. A lower Pr_t value leads to lower rod surface temperatures. Although the standard Pr_t value for air is around 0.9, values between 0.6 and 1.5

can be found in the literature [7]. The presented simulations were performed with $Pr_t=0.6$. Additional research has to be done to justify this choice and fully understand the Pr_t influence on the results.

In order to investigate the influence of the turbulence modeling on the CFD results, SRS calculations were performed for the SH-TX-01 run: one ZLES and one SAS simulation. In the ZLES case the whole CFD domain is divided in two subdomains: a large subdomain which includes the test section and a small one with the test section inlet and the outlet regions. In the first one the WMLES model is selected, while in the second one, the flow is calculated using the two-equation eddy viscosity model SST. The simulation results were averaged over 5 s. Figure 5 visualizes turbulent flow structures colored with velocity (ZLES calculation). The performed fine resolution SRS simulations confirmed the RANS results with the SST turbulence model. Therefore, it is not easy to draw a general conclusion. A simplification has been done by applying constant heat losses in the simulations. These vary in reality over the test section length, but it is not expected that their influence on the results is very large.

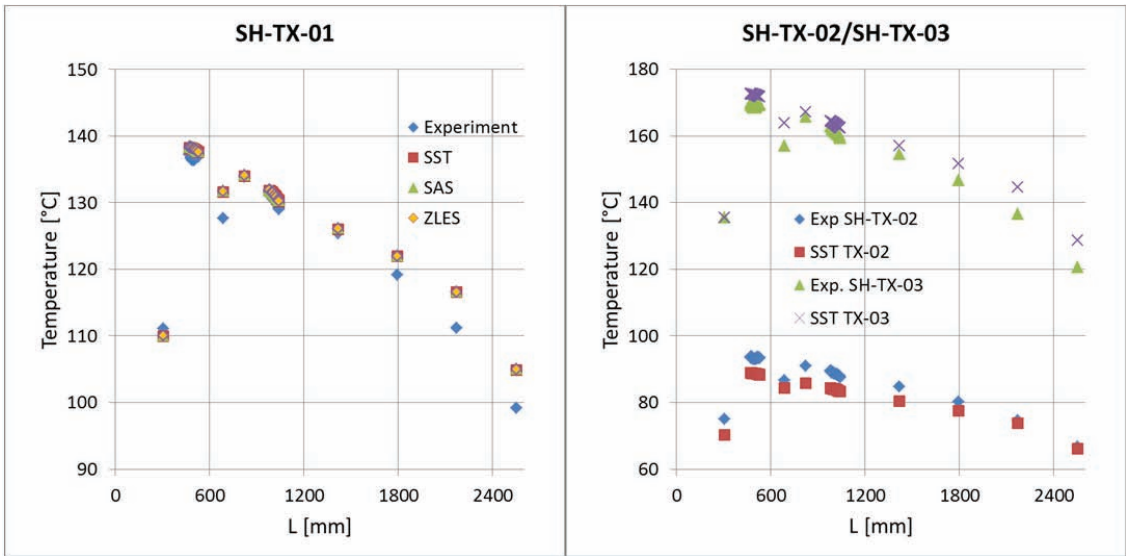


Figure 3. Temperature Profiles for SH-TX-01. Figure 4. Temperature Profiles for SH-TX-02/03.

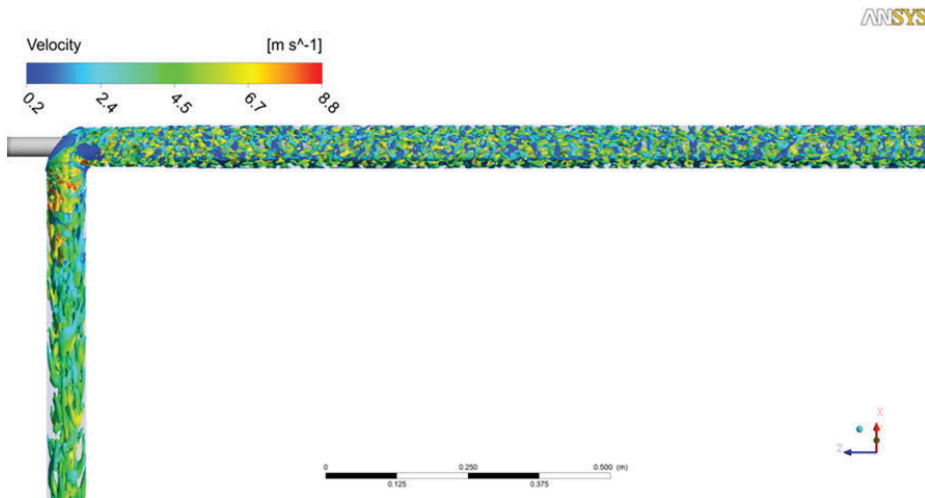


Figure 5. Velocity Colored Turbulent Flow Structures.

4. TALL-3D EXPERIMENT AND ANSYS CFX MODEL DEVELOPMENT

4.1. TALL-3D Facility and T01.09 Experiment

The TALL-3D thermal hydraulic loop is an integral 7 m high experimental facility, operated by KTH [1]. It consists of two fully instrumented circuits. The primary circuit consists of three vertical legs, filled with LBE. In the middle leg, a 3D test section is installed (see Fig. 6, left), which is domain of complex 3D effects and source for challenging TH feedback to the rest of the loop. A heater is wrapped around the upper part of the outer test section wall. This enhances the buoyancy effects in the test section at natural circulation conditions. Inside the test section pool, a metal plate prevents the cold LBE from leaving the vessel without extensive mixing with the heated fluid inside it. In this paper, emphasis is given only to the test section behavior, while the simulation results for the complete facility are discussed in [8]

The TALL-3D facility is well instrumented with thermocouples (TCs). Only in the test section there are more than 140 TCs. Figure 6 (right) shows the location of the main TC groups in the test section: CIP (circular inner plate TCs), BP (bottom plate TCs), IPT (inner pipe TCs), ILW (inner lateral wall TCs), OLW (outer lateral wall TCs). Each TC group can be found four times in the cylindrical pool – at 0°, 90°, 270° and 360°. Since the calculated experiment is symmetric, the average value of each 4 TCs is compared with the prediction of the simulations.

In the TALL-3D T01.09 experiment the main circulation pump is tripped [9]. This leads to a dynamic TH transient in the facility with local 3D phenomena like LBE mixing and stratification which affect the overall loop behavior. T01.09 starts from a steady state forced convection with 1.64 kg/s LBE mass flow rate at 239 °C in the 3D test section leg. The heater power of 4810 W is kept constant during the whole transient. When the pump is tripped ($t=0$ s), the mass flow rate in the 3D test section leg decreases abruptly and even reverses for a short time.

4.2. ANSYS CFX Model of the TALL-3D Facility

Since the TALL-3D experiments are long and therefore require substantial computational effort, a 2D model was generated, representing 1° rotational symmetry sector of the test section. It should be mentioned, that the flow pattern in this transient is symmetric. This mesh was systematically refined and grid sensitivity studies were performed according to the OECD Best Practice Guidelines [2]. The selected final mesh for the 1° simulations has 109.000 elements (Fig. 6, center). The mesh quality is very good with a minimum orthogonally angle of 88°, an expansion factor of 13 and a maximum aspect ratio of 216.

The LBE properties were obtained from the OECD “Handbook on Lead-Bismuth Eutectic Alloy and Lead Properties” [10]. The equations of the fluid properties were implemented in ANSYS CFX using CEL (CFX Expression Language) expressions [11]. For the correct modelling of the buoyant LBE flows in the TALL-3D test section, buoyancy terms in the momentum equation and in the production terms of the turbulence model equations have been included. All calculations presented here were performed with the SST turbulence model [3]. In the transient CFD simulations, Second Order Backward Euler transient scheme was selected, while for the numerical transport of the quantities (velocity, temperature, etc.) through the solution domain a High Resolution advection scheme was used. An adaptive time stepping (time step size between 0.05 and 0.1 s) was specified in the CFD simulations. Measured T01.09 data was imposed as transient boundary conditions at the inlet (mass flow rate, temperature) and outlet of the test section (temperature). At the inlet a flat velocity profile 10 % turbulence intensity were imposed. The length of the test section inlet pipe allows the turbulent velocity profile to develop, before the LBE enters the pool. Monitor points were positioned in the test section at the TC locations.

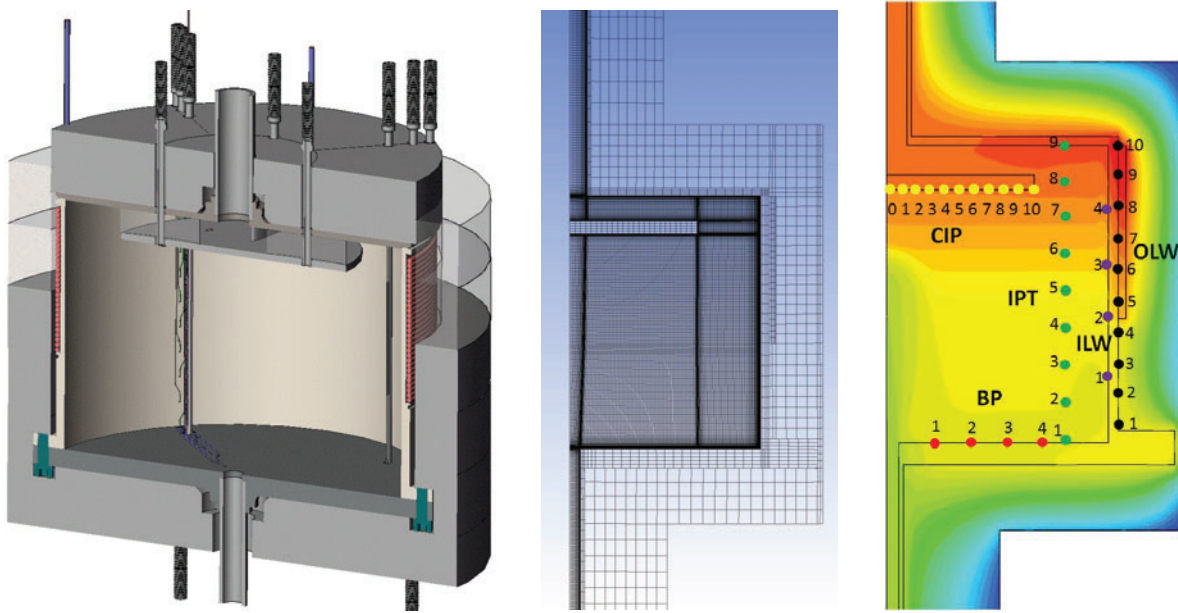


Figure 6. TALL-3D Test Section (left), Hexahedral Mesh (center) and Position of the TC Groups (right).

5. ANSYS CFX VALIDATION AND DISCUSSION ON THE TALL-3D RESULTS

In the following paragraphs the results for the main 3D test section TC groups are analyzed and compared with data [12]. The measurement uncertainty of the installed TCs in TALL-3D provided by KTH is 1.5 K. Since the total number of all TCs exceeds 140, only representative TCs from each group are shown. For a better understanding of the following results, the reader is referred to Fig. 6 (right) for the description of the location of the discussed TCs. The simulated transient time is 5000 s. In order to have better temporal resolution in the transient phase, only 2500 s are shown here. The observed deviations between experiment and calculation at $t=2500$ s do not increase thereafter.

5.1. Velocity and Temperature Distributions

In order to better understand the transient T01.09, velocity and temperature fields were plotted at selected transient simulation times. One should keep in mind, that the color scaling in each picture is different. It is chosen with respect to the minimum and maximum values of the quantities for the selected plane and transient time. This allows better color resolution and flow visualization.

Figure 7 shows the velocity distribution at $t=0$ s just before the initiation of the transient. It can be seen that at forced circulation conditions the LBE jet impinges on the inner circular plate and then detaches from the plate. Large amount of the detached LBE sloshes on the side wall, forming three large eddies in the CFD domain. The central one rotates in clockwise direction and removes heat from the side test section wall. The hot LBE is then transported to the central and lower pool regions, where it is mixed with the cold LBE. Small part of the detached LBE from the plate flows upwards, rotating in counter-clockwise direction. This swirl cools down the upper right corner of the pool, where the heater ends. As a consequence of the high mass flow rate and pool geometry, the T01.09 forced circulation steady state leads to a fully mixed flow pattern in the 3D test section pool (see Fig. 8). Figures 9 and 10 represent the

LBE flow pattern at steady state natural circulation conditions ($t=2500$ s). At low velocities and with heater still switched on, buoyancy effects play an important role and thermal stratification is established in the CFD domain. Cold and heavy LBE stratifies at the bottom of the test section, while lighter, hot LBE can be found in the upper half of the test section pool. The maximum velocity occurs in the test section inlet pipe, while the maximum temperature is found in the top right corner of the test section pool.

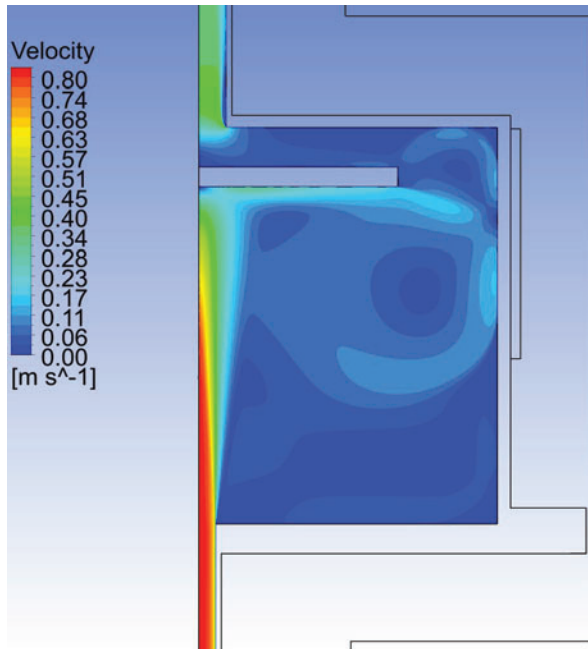


Figure 7. Velocity Distribution at $t=0$ s.

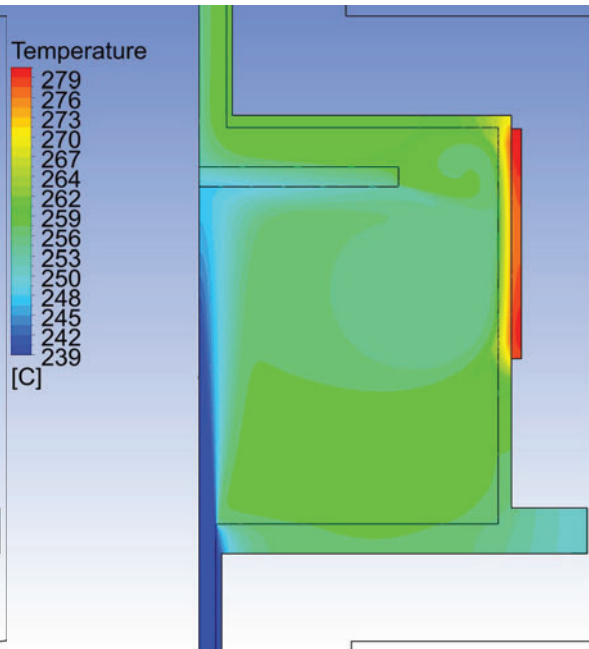


Figure 8. Temperature Distribution at $t=0$ s

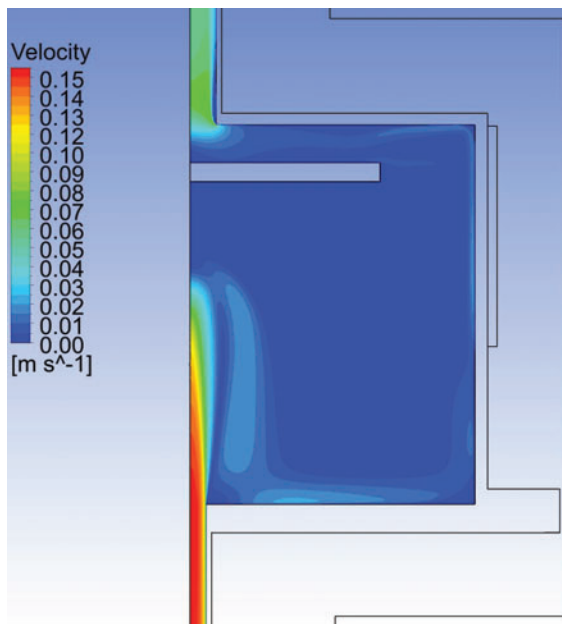


Figure 9. Velocity Distribution at $t=2500$ s

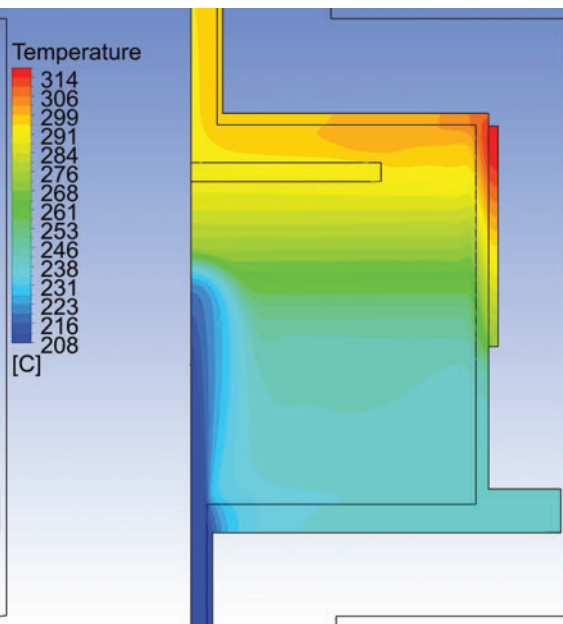


Figure 10. Temperature Distribution at $t=2500$ s

5.2. Comparison of Calculated and Experimental Data

5.2.1 Main inlet and outlet temperatures

The temperature at the inlet (see Fig. 11) is a boundary condition in this calculation almost for the whole transient. Between $t=95$ s and $t=198$ s transient time the flow in the test section reverses and therefore the temperature at the inlet is calculated by the CFD code. It can be seen, that in this period the calculation overestimates the experiment by max. 4 K. This means that the LBE temperature in the vicinity of the pool bottom plate is higher, than the one observed in the experiment. One possible reason for this is slight overestimation of the mixing in the pool. In a well-mixed pool, the hot LBE from the upper pool part will be mixed with the colder one, which is close to the pool bottom. The main outlet temperature calculated with ANSYS CFX agrees well with the experiment (Fig. 11). The first temperature peak is captured very good. Thereafter, in the time frame 800-2000 s, a systematic underestimation of the temperature by max. 3 to 4 K can be observed. With transient progression this deviation decreases.

5.2.2 Bottom plate temperatures (BP1...4)

All four bottom plate TCs show similar behavior and good agreement with the experiment. Figure 12 presents the simulation and experimental results for TC BP1 (close to the inlet pipe) and BP4 (close to the side wall). It can be seen that there is a very good agreement for the first part of the transient, while after 1200 s a slight overestimation of the temperature appears. Still, the maximum deviation from experiment lies, however, within 2.5 K.

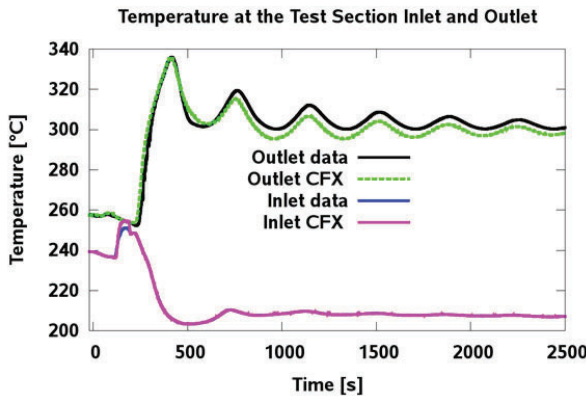


Figure 11. Temperature at Inlet and Outlet.

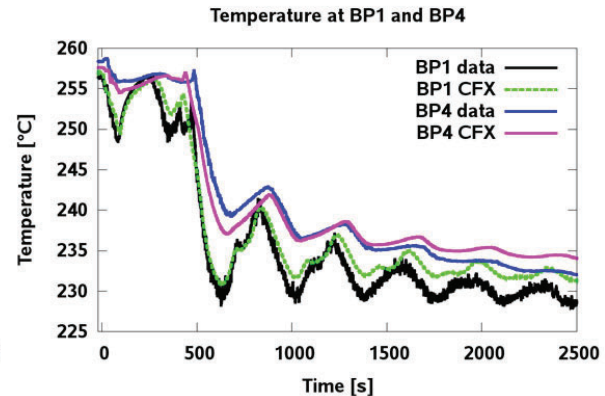


Figure 12. Bottom Plate Temperatures.

5.2.3 Inner pipe temperatures (IPT1...9)

The nine IPT TCs can be found inside the pool, between the inner plate and the wall. IPT1 is positioned almost at the pool bottom, while IPT9 is close to the top of the pool. The IPT TCs give a good picture of the flow behavior inside the pool in axial direction. The calculation results show good agreement with measured data (see Fig. 13 and Fig. 14). The axial profile in the test section pool is well captured at forced circulation. Discrepancies up to 3.5 K from data can be observed in the lower pool part at natural circulation. The observations made for the BPs are valid here as well – the CFD calculation shows slightly warmer fluid in the lower pool part at natural circulation conditions. In the middle and upper parts of the test section pool a very good agreement with experimental data exists.

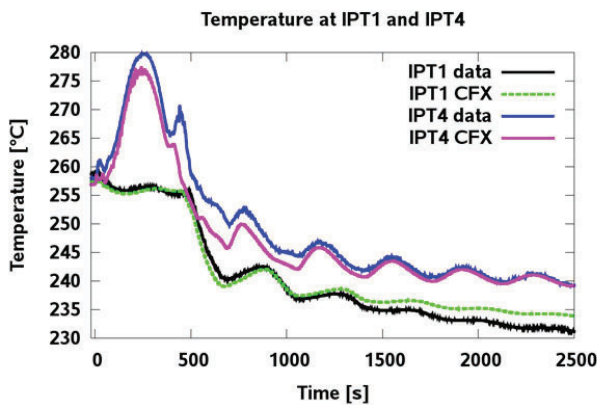


Figure 13. Inner Pipe Temperatures.

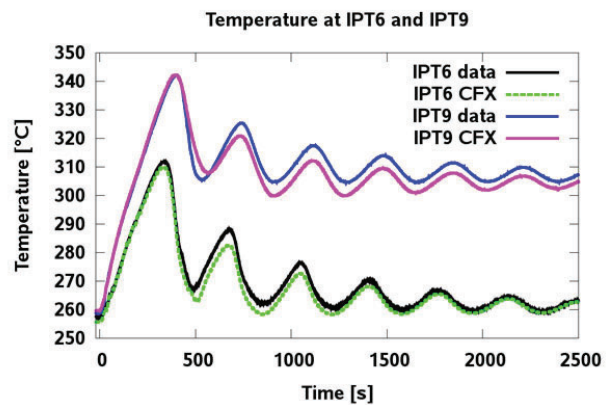


Figure 14. Inner Pipe Temperatures.

5.2.4 Inner lateral wall temperatures (ILW1...4)

The ILW TCs are attached to the inner pool wall. The trend from the previous TCs is observed here as well: the CFD code predicts slightly warmer fluid (by 2-3 K) in the lower pool part, while in the top part the agreement is very good. Figure 15 and Fig. 16 depict the comparison of measured and calculated data for ILW1, ILW2, ILW3 and ILW4.

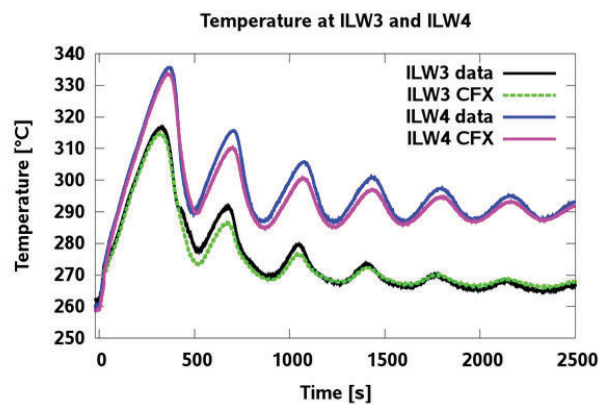
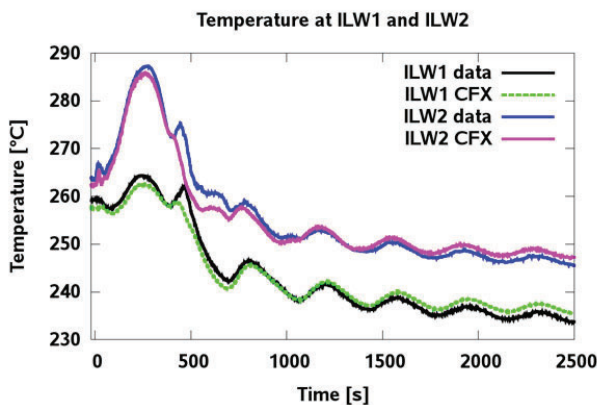


Figure 15. Inner Lateral Wall Temperatures. Figure 16. Inner Lateral Wall Temperatures.

5.2.5 Outer lateral wall temperatures (OLW1...10)

Good overall agreement can be observed also for TCs OLV1, OLV3, OLV6 with deviations from the experimental data within the range 2-4 K (see Figures 17 and 18). All these TCs are installed on the lower part of the side wall surface. OLV9 is in the upper part of the side wall, just between the wall and the heater. The deviation here lies within 15 K. Subsequent analyses on the experimental data revealed some inconsistencies associated with the OLV values in the heater region.

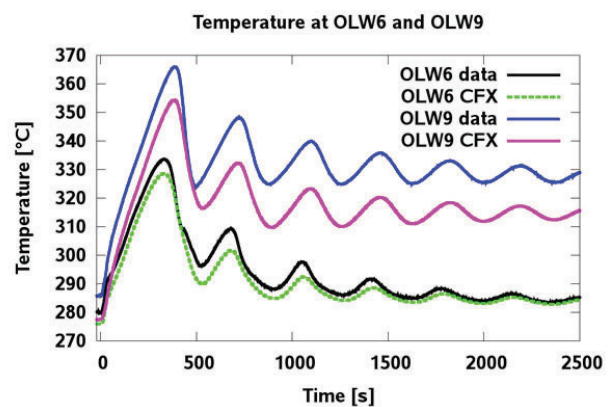
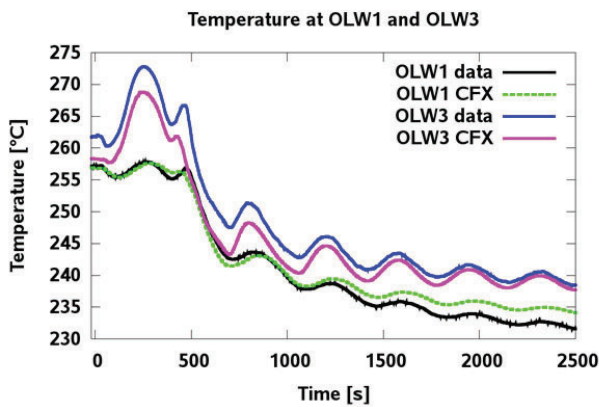


Figure 17. Outer Lateral Wall Temperatures. Figure 18. Outer Lateral Wall Temperatures.

5.2.6 Circular inner plate wall temperatures (CIP0...10)

These TCs are positioned on the lower surface of the circular inner plate. CIP0 (Fig. 19) is located in the very center of the plate, while CIP10 (Fig. 20) is positioned at its outer edge. CIP6 is almost in the middle between CIP0 and CIP10. The low temperature peaks at simulation time $t \sim 380$ s (see Fig. 19) appear, because the oscillating cold LBE jet impinges on the plate (Fig. 21). The first two CIP0 peaks are captured very well by the CFD code, while the temperature of the third peak is overestimated. Next peaks are small, but still not captured by the code. In the case of CIP3 (Fig. 19), the second peak is already missed in the simulation. The agreement for CIP6 (Fig. 20) is good, except for the missing first low peak in the calculation. The same is valid for CIP10, but such peak is not present, because this TC is far away from the front of the LBE jet. One can conclude that the exact shape of the impinging jet is not precisely captured by the calculation. However, it is well known, that impinging jets represent a major challenge for the two-equation eddy viscosity turbulence models. Moreover, the 2D mesh represents an additional constraint for its proper simulation. An adequate simulation of impinging jet requires the utilization of advanced turbulence techniques. SRS such as LES, ZLES or SAS together with 3D CFD meshes (90° or larger symmetry sectors) would be more appropriate for the prediction of flows with impinging jets. Such simulations are currently being performed at GRS.

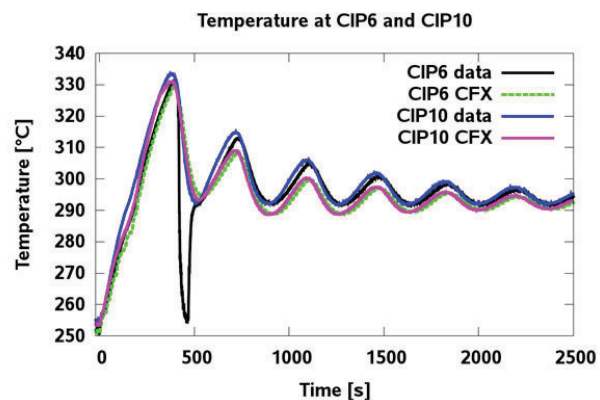
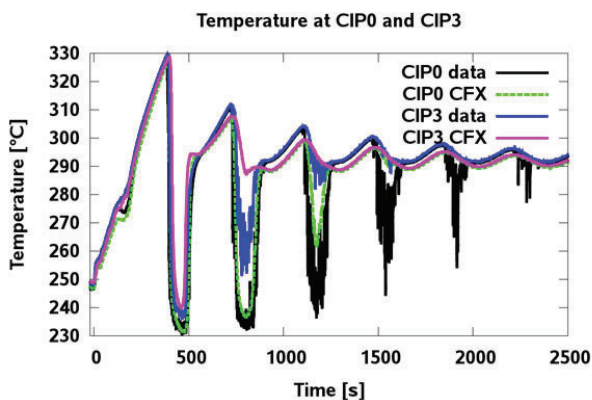


Figure 19. Circular Inner Plate Temperatures. Figure 20. Circular Inner Plate Temperatures.

6. IMPORTANCE OF THE CONJUGATE HEAT TRANSFER MODELING IN T01.09

Figures 8 and 10 show the temperature distribution in the test section at forced and natural circulation conditions. Temperature gradients in the solid walls, heater and the metal plate inside the pool can be observed. It turned out, that the consideration of this conjugate heat transfer (CHT) is very important for the CFD results. First TALL-3D calculations were performed with a fluid domain only. A constant wall heat flux, based on the specified heater power, was imposed as boundary condition on the fluid surface. Because of the constant heat flux during the whole transient, this approach led to overestimation of the temperatures inside the domain (see Fig. 21). Moreover, since the T01.09 transient was designed to be dynamic, the amplitude and the frequency of the temperature fluctuations could not be resolved accurately in the simple CFD simulation, because of the missing solid metal mass. Solid walls introduce thermal inertia, which is of great importance for the transient dynamics. This was also confirmed by the simulation results of further TALL-3D experiments.

In reality the heat flux varies, since it is a function of the heater power, LBE velocity and temperature, and the thermal properties of the LBE and the solid metals (test section wall, heater). With the presented extended TALL-3D model the CHT phenomena were considered through explicit solid wall modeling and specification of a volumetric power inside the heater domain. The current TALL-3D model takes into account even the behavior of the thermal insulation around the test section (see Fig. 6, right). It was also found that the metal plate inside the test section is responsible for a remarkable heat transfer between the cold fluid below this plate and the hot fluid leaving the test section pool. The cold LBE impinges on the lower plate surface plate and through heat conduction in the solid metal cools the hot LBE leaving the test section. This is well seen in Fig. 22, but might be observed also in Fig. 8.

The previous observations lead to the conclusion that CHT must be considered for transient flows in order to obtain high quality CFD results. Solid structures need significantly lower mesh resolution in comparison to the fluid part of the computational domain. Therefore, a small increase in the computation time can be expected. Moreover, with the additional solid domain the TALL-3D simulations converged as fast as the ones without it.

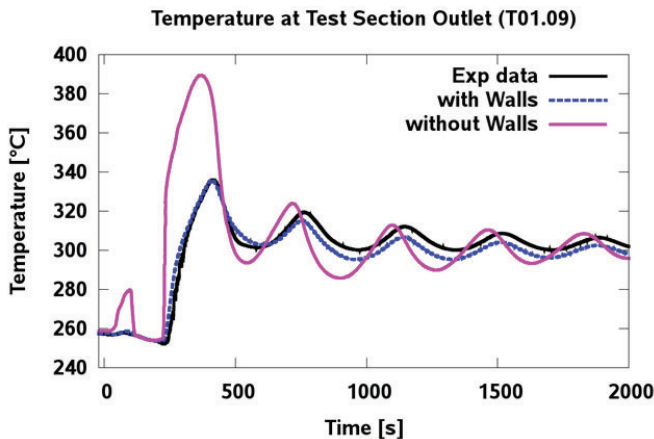


Figure 21. Outlet Temperature Calculated with and without Consideration of the Metal Structures in the Test Section.

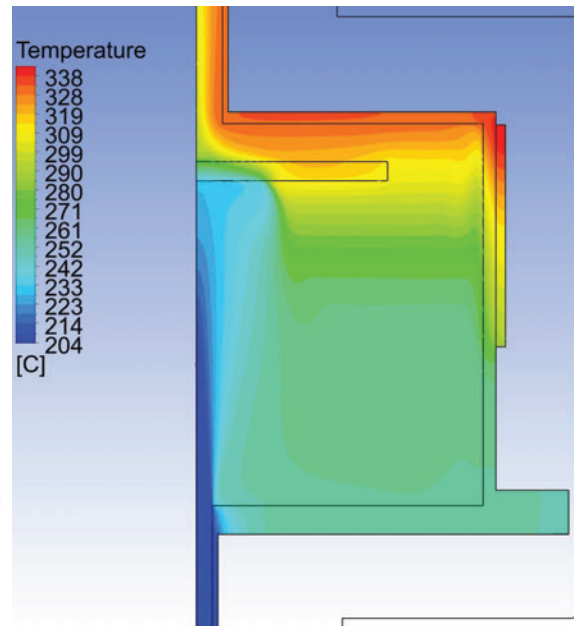


Figure 22. Reduction of the Outlet Temperature through CHT in the Circular Inner Plate.

7. CONCLUSIONS

Steady state RANS and transient LES and SAS calculations were performed for five L-STAR experiments with heated smooth rod. Good results for the pressure drop along the test section as well as for the outlet temperature have been achieved. The prediction of the temperature distribution along the heated rod surface turned out to be more challenging. Calculated and measured data are in good agreement and revealed the capability of ANSYS CFX to predict correctly the gas flow pattern in the L-STAR experiments. Nevertheless, some deviations up to 8 K were observed at different locations in the different experimental runs. In order to better understand these discrepancies, fine resolution ZLES and SAS simulations were performed. These only confirmed the RANS results with the SST turbulence model. Therefore, further analyses are needed to fully understand the flow in the L-STAR experiments. Additional work is required to investigate the influence of the turbulent Prandtl number Pr_t , which turned out to be an influential parameter.

The numerical results obtained with ANSYS CFX for the TALL-3D T01.09 experiment show that the code is capable to capture qualitatively and quantitatively the main TH phenomena occurring in the test section. LBE mixing and stratification, buoyancy effects and the transition from forced to natural circulation in the facility were predicted correctly by the CFD simulation. Good agreement has been observed for all TC groups, the deviations from experimental data are less than 6 K. The 2D axisymmetric CFD models provided good results for the most of the TCs. One should not forget that T01.09 is a symmetric transient and this approach will not work for asymmetric 3D flows. Moreover, the impinging jet area (CIPs) is not resolved correctly by the CFD code. Larger TALL-3D models (90° sector or full CFD model) would allow the utilization of advanced turbulence models such as LES, ZLES, SAS, etc.

Finally, for high quality CFD results, solid metal components need to be modelled. These allow the consideration of CHT, which appears to be an important phenomenon, especially in transient calculations, where the thermal inertia of the metal structures needs consideration.

ACKNOWLEDGMENTS

This work was supported by the EC 7th Framework Project THINS (Thermal-Hydraulics of Innovative Nuclear Systems, Grant No. 249337) and partly financed by the German Federal Ministry for Economic Affairs and Energy.

REFERENCES

1. R. Gomez, R. Krüssmann, M. Böttcher, F. Arbeiter, W. Hering, "Experimental investigation of heat transfer and pressure drop for turbulent air flows in hexagonal channels", Proceedings of the ICONE-21 Conference, Chengdu, China, July 29 – August 2, 2013
2. OECD/NEA, "Best Practice Guidelines for the use of CFD in Nuclear Reactor Safety Applications", NEA/CSNI/R(2007)5, 2007.
3. F. Menter, "Two-Equation Eddy-Viscosity Turbulence Models for Engineering Applications", AIAA-Journal, **32**, pp. 269 – 289 (1994).
4. ANSYS, "ANSYS CFX 14.5 User's manuals", 2012.
5. F. Arbeiter, J. Aberle and M. Böttcher, THINS Del.1.1.07 "Progress report on experimental L-STAR results" KIT, Karlsruhe, Germany, 2013.
6. S. Buchholz, THINS Del. 1.1.10 "Report on SAS and LES modelling and comparison to single rod L-STAR data" GRS, Garching, Germany, 2013.

7. D. A. Anderson, J. C. Tannehill and R. H. Pletcher, "Computational Fluid Mechanics and Heat Transfer", New York: Hemisphere Publishing Cooperation, 1984.
8. A. Papukchiev, C. Geffray, M. Jeltsov, K. Kööp, P. Kudinov, D. Grischenko "Multiscale Analysis of Forced and Natural Convection Including Heat Transfer Phenomena in the TALL-3D Experimental Facility", Proc. of the NURETH-16 Conference, Chicago, USA, August 30, September 4, 2015.
9. D. Grishchenko, M. Jeltsov, K. Kööp, A. Karbojian, W. Villanueva, P. Kudinov "The TALL-3D Facility Design and Commissioning Tests for Validation of Coupled STH and CFD Codes" Nuclear Engineering and Design, In Press, available online 11 February 2015.
10. OECD/NEA, "Handbook on Lead-Bismuth Eutectic Alloy and Lead Properties, Materials Compatibility, Thermal-hydraulics and Technologies" NEA No. 6195 (2007)
11. A. Papukchiev and G. Lerchl, "Extension and Application of the Coupled 1D-3D Thermal-Hydraulic Code ATHLET-ANSYS CFX for the Simulation of Liquid Metal Coolant Flows in Advanced Reactor Concepts", Proc. of the ICONE-20 Conference, Anaheim, USA, July 30 - August 3, 2012
12. A. Papukchiev and C. Geffray, THINS Del.5.2.03 "Multiscale Calculation Results on TALL-3D" GRS/TUM, Garching, Germany, 2015.